Sensors & Actuators: B. Chemical 358 (2022) 131486

Contents lists available at ScienceDirect

Sensors and Actuators: B. Chemical

journal homepage: www.elsevier.com/locate/snb

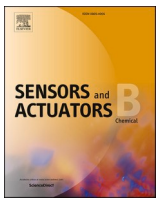

Selective photoactive gas detection of CO and HCHO using highly porous SnO_2 and SnO_2@TiO_2 heterostructure

Sungjin Kim [a,b,1], Deok-Hyun Cho [a,b,1], Hyeon-Kyung Chang [a,b], Ho-Nyun Lee [a], Hyun-Jong Kim [a], Tae Joo Park [b,*], Young Min Park [a,*]

[a] Surface Technology Group, Korea Institute of Industrial Technology (KITECH), Incheon 21999, South Korea
[b] Department of Materials Science and Chemical Engineering, Hanyang University, Ansan 15588, South Korea

ARTICLE INFO

Keywords:
Photoactive gas sensors
Carbon monoxide
Formaldehyde
Porous heterostructure
Thermal evaporation
Atomic layer deposition

ABSTRACT

Herein, a controlled porous structure for photoactive gas sensors was fabricated using the gas-flow thermal evaporation and atomic layer deposition method. To control the porosity of the SnO_2 matrix, Ar was introduced to the chamber to adjust the pressure from 0.1 to 1 Torr during thermal evaporation. Furthermore, nanoscale TiO_2 layers were conformally deposited on the surface of porous SnO_2 by atomic layer deposition as a selective active layer for HCHO. As a result, the sensor deposited at a pressure of 0.2 Torr showed high sensitivity and a relatively fast response than other deposition pressures owing to the optimized porosity and better electron transport. The nanoporous structure of SnO_2 showed a high response rate of 56.7% when exposed to CO with a concentration of 50 ppm and a low detection limit of 1 ppm. The introduction of a TiO_2 layer on the nanoporous SnO_2 allowed selective response to HCHO with a response rate of 20% at 10 ppm when the oxidation level of the target gas was well aligned with the state of reactive oxygen of materials under UV irradiation. Furthermore, the sensing capabilities of the SnO_2 and SnO_2@TiO_2 heterostructures, such as the response rate and response time, were assessed at different deposition pressures. Our results clearly show that the matching of energy levels between the redox energy of the target gas and the conduction band of the materials plays an important role in selectively detecting the target gas in photoactive gas sensors; therefore, we propose a rational design rule to enhance the selectivity for various target gases.

1. Introduction

Chemiresistive gas sensors have been widely studied for practical applications such as public safety, indoor and industrial air monitoring, and environmental diagnostics [1]. For practical applications of gas sensors, it is necessary to monitor the concentration of each gas and distinguish the type of gas from an alarm to the user [2]. In the past few decades, metal oxide semiconductors, such as SnO_2, [3,4] TiO_2, [5,6] ZnO, [7,8] WO_3 [9,10] and CeO_2 [11] have been widely investigated for gas sensing of various toxic gases. Metal oxide semiconductor-based gas sensors are known to offer advantages such as high response, good stability, and rapid response toward target gases with low cost and easy fabrication methods. Nonetheless, high-temperature operation over 200 °C, which is required to generate oxygen species for reaction with the target gas in metal oxides, still limits the wide applications of gas sensors [12]. The high operating temperature of conventional gas sensors induces instability and a short lifetime resulting from the change in grain size and microstructure, and it also results in high power consumption and long warm-up time [13]. Recently, several studies have attempted to reduce the operating temperature and working power of metal oxide-based gas sensors using novel metal doping structures [14–16], core/shell morphologies [17], manufactured electrostatic fields [18], and controlled the micro/nano size of metal oxide to increase the active area of target gases [19,20]. Among these methods, photoactive gas sensors, which take the advantage of UV irradiation to generate reactive oxygen species, have been considered as a promising and alternative way to enhance sensing properties with low operation temperature and power consumption [20–22]. Because the electron-hole pair produced under UV irradiation produces reactive oxygen species on the surface of the semiconductor, the photoactive gas sensor can be operated near room temperature and achieve a short warm-up time. Many research efforts have concentrated on the enlarged

* Corresponding authors.
E-mail addresses: tjp@hanyang.ac.kr (T.J. Park), youngmin@kitech.re.kr (Y.M. Park).
[1] These authors equally contribute this work.

https://doi.org/10.1016/j.snb.2022.131486
Received 5 July 2021; Received in revised form 5 January 2022; Accepted 24 January 2022
Available online 26 January 2022

active surface area for higher sensitivity and the combination of material synthesis to achieve gas selectivity [23–26]. Most fabrication methods, however, have taken advantage of solution-based methods, which retain organic surfactants and binder residues during the synthesis processes, thereby reducing the active surface area and reducing the response to gas. Furthermore, depending on the selection of materials, solution-based fabrication and surface modification of porous structures are limited; hence, a more reliable fabrication method for porous heterostructures is required to achieve high sensitivity and versatility to various target gases.

In this study, a highly porous heterostructure of SnO_2 for sensing carbon monoxide (CO) and SnO_2 @TiO_2 for sensing formaldehyde (HCHO) was demonstrated by gas-flow thermal evaporation and atomic layer deposition (ALD). By changing the deposition pressure with Ar gas flow from 0.1 to 1 Torr during thermal evaporation, the porosity of SnO_2 was controlled, and the consequential gas-sensing properties with operating pressures were compared at room temperature (27 °C). Therefore, at an Ar pressure of 0.2 Torr, the porous structure shows the best performance for gas-sensing properties, such as high response rate and time to CO gas, with a concentration range of 50–1 ppm, owing to the trade-off between the active surface area and charge transport. The introduction of a conformal TiO_2 layer, which is known as the redox energy of HCHO, has been shown to result in the specific sensing of HCHO, maintaining the performance of gas-sensing properties. The stability of our sensors was also investigated under various humid conditions and the injection of other gases.

2. Experimental method

2.1. Preparation of highly porous SnO_2 and SnO_2@TiO_2 gas sensors

The SnO_2 films were prepared using a modified gas-flow thermal evaporation system of chamber-type (ULTEC) with different vapor pressures from 0.1 to 1 Torr to control the porosity, as reported previously [27]. Tin monoxide (SnO) granules (0.2 g, 99.995% pure, LTS Research Laboratories, Inc., USA) were used as source material. The evaporation was carried out in a turbo pump vacuum system operated at 5×10^{-6} Torr of vacuum pressure, which was filled with Ar gas up to constant pressures of 0.1, 0.2, 0.5, and 1 Torr with a flow of 100 sccm. During the deposition process, the substrate was maintained at 23 °C using a cooling system. After deposition, the substrates were annealed in a tube furnace at 700 °C under an air atmosphere for 1 h to convert to the SnO_2 crystallite structure [28–30]. The TiO_2 layers were deposited on the porous SnO_2 sensor by an ALD system using titanium tetraisopropoxide (TTIP) (UP Chemical Co. Ltd., Korea) and deionized (DI) water as the precursor and reactant, respectively. The stage temperature was maintained at 300 °C, and 200 ALD sequence cycles were performed to deposit a 2 nm TiO_2 layer.

2.2. Characterization of SnO_2 and SnO_2@TiO_2 sensors

X-ray diffraction (XRD) patterns of the porous SnO_2 thin films prepared at different deposition pressure conditions were analyzed using an X′Pert PRO MPD (PANalytical, NLD) with Cu Kα radiation in the range of $2\theta = 20–60°$ at a scanning rate of 5°/min, and the patterns were indexed with standard data (JCPDS file. 41–1445). The microstructure and morphology of SnO_2 and SnO_2 @TiO_2 were also investigated using field emission scanning electron microscopy (FE-SEM) images using a JSM-7100 F microscope (JEOL, USA) operating at 30 kV. Samples for transmission electron microscopy (TEM) were prepared by dispersing the powders in ethanol and depositing a few drops of the dispersion solution on a carbon grid. TEM images were obtained at 200 kV using a Tecnai G2 F20 microscope (FEI, NLD).

2.3. Gas-sensing measurement

The interdigitated electrodes for photoactive gas sensors were patterned with dimensions of length and width of 4 and 10 μm, respectively, on a 300-nm thick Si_3N_4/Si wafer. As electrode materials, 50-nm-thick Ti and 200-nm-thick Pt were successively deposited. Highly porous SnO_2 and SnO_2@TiO_2 morphologies were deposited on the as-fabricated interdigitated Pt electrode by thermal evaporation at different Ar vapor pressures. A 275-nm UV-LED array (SeoulVIOSYS) was used to measure the gas-sensing properties at room temperature (27 °C). We estimated the gas-sensing properties of SnO_2 and SnO_2@-TiO_2 to CO and HCHO gases under UV irradiation with a light intensity of 150 and 50 μW/cm^2, respectively. Gas sensing under UV light activation was measured using a source meter (Keithley 2636A) at a constant voltage. We measured the resistance change of photoactive gas sensors when exposed to CO gas at concentrations of 2, 5, 10, 30, and 50 ppm and HCHO gas at concentrations of 0.1, 0.5, 1, 3, 5, and 10 ppm. Moreover, we estimated the gas-sensing behaviors of SnO_2 and SnO_2@TiO_2 porous structures at various humidities (35%, 50%, and 80%), which were controlled by introducing deionized water vapor through a bubble system mixing dried gas. We calculated the response of the gas sensors using the equation $[(R_a\text{-}R_g)/R_a \times 100\%]$, where R_a is the resistance of the sensor in air and R_g is the targeted gas [14]. The response time was obtained using the time required to achieve 90% from 10% of the total resistance change upon adsorption.

3. Result and discussion

3.1. Characterization and CO sensing properties of porous SnO_2 sensor

Highly porous SnO_2 and SnO_2@TiO_2 heterostructures were obtained by the gas-flow thermal evaporation and ALD methods with control over the porosity for the selective detection of CO and HCHO gas, respectively (Fig. 1). The introduction of Ar gas with a pressure range of 0.1–1 Torr induces the loss of kinetic energy and the coalition of evaporated atoms, thus allowing for a controlled porous structure [27,31]. Furthermore, the conformal coating on the porous structure by ALD enables the surface of materials to selectively respond to specific gases. The scanning electron micrograph (SEM) images show that the size of the porous structure decreases with increasing Ar pressure from 0.1 to 1 Torr, while the thin film of SnO_2 is well deposited under a high vacuum (Fig. 2). The cross-sectional image also shows that the controlled porous structure is uniformly deposited on the substrate. The XRD patterns of the as-synthesized porous SnO_2 were indexed in good agreement with the standard JCPDS card 41–1445 with a tetragonal structure (Fig. S1) [32, 33]. The corresponding active surface areas of porous SnO_2 deposited at 0.1, 0.2, 0.5, and 1 Torr were measured using Brunauer–Emmett–Teller (BET) analysis as 50.1, 63.9, 68.9, and 71.6 m^2/g, respectively. (Fig. S2) These results show that the controlled porous SnO_2 has a large specific surface area and abundant nanosized pore interface structure. The increased surface area with processing pressure is mainly because of

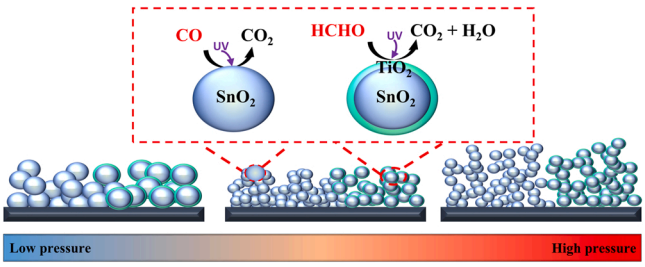

Fig. 1. Schematic of photoactive gas sensors based on the porous SnO_2 and SnO_2@TiO_2 structure by gas-flow thermal evaporation deposition and atomic layer deposition.

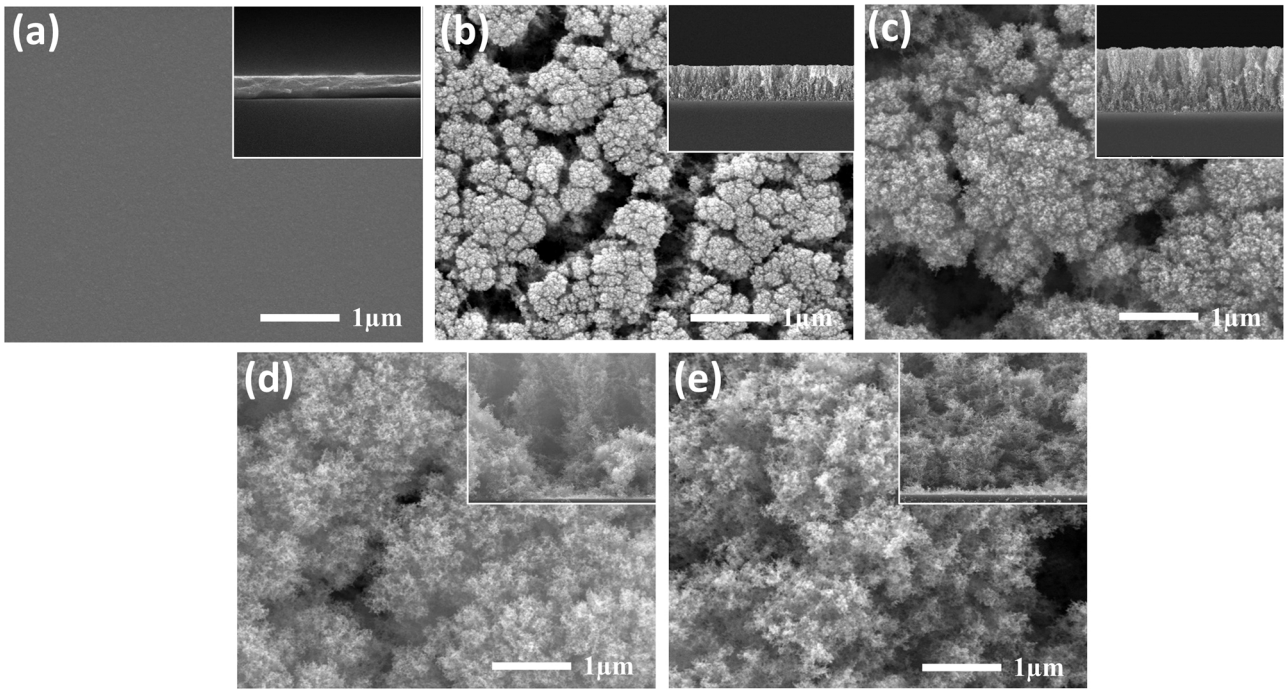

Fig. 2. FE-SEM images of porous SnO_2 surface with different thermal evaporation deposition pressure: (a) high vacuum, (b) 0.1 Torr (0.1SnO), (c) 0.2 Torr (0.2SnO), (d) 0.5 Torr (0.5SnO) and (e) 1 Torr (1SnO) (inset: cross-sectional images of porous SnO_2 on substrate, 100 k magnification).

lower kinetic energy of evaporated atom leading to form the smaller particle size as reported previously [27]. High-magnification transmission electron microscopy (TEM) images show that a particular structure is formed with a size less than 20 nm regardless of the deposition pressure, which indicates that the deposition pressure mainly affects the density of SnO_2, thereby changing the porous structure (Fig. S3).

The photoactive gas-sensing properties of the as-synthesized highly porous SnO_2 structure at different Ar pressures of 0.1 (0.1SnO), 0.2 (0.2SnO), 0.5 (0.5SnO), and 1 Torr (1SnO) were estimated at different concentrations of carbon monoxide (CO) from 50 to 2 ppm under UV irradiation with UV-LED at room temperature (Fig. 3). The effect of UV light intensity on the response to CO gas (30 ppm) is estimated with porous SnO_2 deposited at Ar pressure of 0.2 Torr and light intensity of 10–300 μW/cm^2 (Fig. S4). Although increasing light intensity leads to a higher response owing to more exciton generation, the difference in response between 150 and 300 μW/cm^2 is less than 5%; thus, the optimal light intensity is set as 150 μW/cm^2 for CO gas detection considering the sensitivity and power consumption. The dense film of SnO_2 deposited at high vacuum showed less than 10% resistance change upon exposure to 50 ppm of CO. The responses of 0.1SnO, 0.2SnO, 0.5SnO and 1SnO to 50 ppm of CO gas were measured as 37.3%, 56.7%, 26.9% and 29.8%, respectively. The dense SnO_2 sensor showed response change of less than 3% at CO concentration of 2 ppm; however, 0.2SnO showed a resistance change of 18%, which was six times higher than that of the dense SnO_2 structure. This result indicates that the porous structure is advantageous for the detection of the target gas because of its large active surface area. Note that 0.2SnO shows the best response rate, that is, 56.7% and 18% to 50 and 2 ppm of CO, respectively, despite the lower porosity compared to 0.5SnO and 1SnO. This result indicates that there is trade-off of porous structure between electron transport and large surface area that plays an important role in gas-sensing properties. As shown in Fig. 3, 0.2SnO displays a magnitude resistance of the order of 10^5, which is two orders of magnitude lower than that of 0.5SnO and 1SnO. In a highly porous structure with a lower resistance, such as 0.5SnO and 1SnO, it is difficult to transfer electrons during CO oxidation because of the long electron pathway to the electrode. Furthermore, the defect generated on the surface acts as trapping for electron transport,

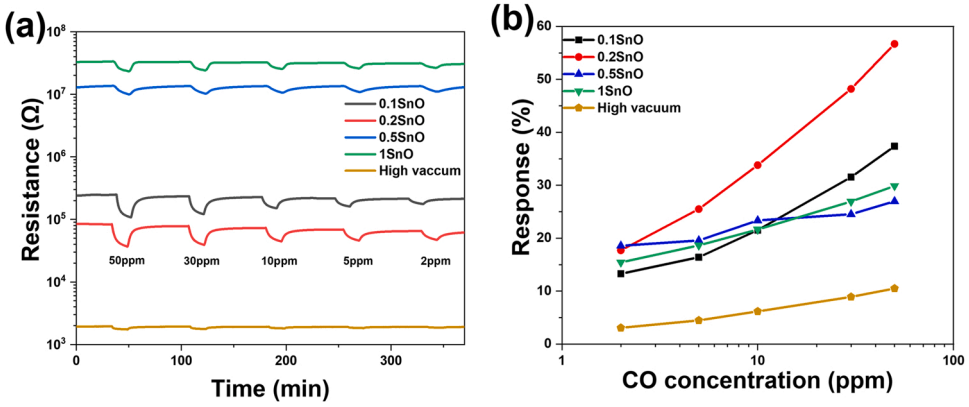

Fig. 3. (a) Transient response of porous SnO_2 gas sensor with different CO gas concentrations from 50 to 2 ppm with various pressure conditions and (b) response properties of porous SnO_2 sensor under UV-LED light (150 μW/cm^2).

thus resulting in a lower sensitivity and response rate.

3.2. Characterization and HCHO sensing properties of SnO_2@TiO_2 sensors

To selectively detect HCHO gases, a thin layer of TiO_2 was conformally deposited on the porous SnO_2 matrix because the TiO_2 band level was well aligned with the redox energy level of formaldehyde (HCHO). Fig. 4 shows the microstructure of the as-obtained SnO_2 templates, which maintain highly porous structures after 200 ALD cycles for the deposition of TiO_2 (Fig. S5(c)). The elemental distribution of Ti in the images obtained from energy-dispersive X-ray spectroscopy clearly shows the TiO_2 are well deposited to the bottom of the pore structure. High resolution TEM images exhibit that TiO_2 layer are well coated on the surface of SnO_2 with a thickness range of 2.2–2.4 nm. (Fig. S6) Electron energy loss spectroscopy (EELS) analysis also revealed that Ti uniformly covered the region with Sn and O elements distributed throughout the entire region, indicating that the TiO_2 layer is conformally coated on the surface of the porous SnO_2 structure with a thickness of ~2 nm (Fig. 5). The gas-sensing properties of the SnO_2@-TiO_2 heterostructure to HCHO were assessed at room temperature under UV irradiation. As shown in Fig. 6, the photoactive gas sensor based on SnO_2@TiO_2 heterostructure on the porous SnO_2 deposited at the pressure at different Ar pressure of 0.1 (0.1TiO), 0.2 (0.2TiO), 0.5 (0.5TiO), and 1 Torr (1TiO) displays well assigned sensing property to HCHO and good linearity with a concentration range of 10–0.1 ppm. While the dense film of SnO_2@TiO_2 deposited under high vacuum conditions displays a low detection response of up to 20% to 10 ppm and 3.2% to 0.1 ppm, the controlled pressure of SnO_2@TiO_2 sensors showed a better response rate (more than 10% to 0.1 ppm)), although 0.5TiO and 1TiO showed a higher response to HCHO; the response and recovery times were slower than those of the other samples, such as 0.1TiO and 0.2TiO, due to slow charge transport. In Fig. 6, 0.2TiO shows not only a faster recovery time but also a higher response rate at a low concentration of HCHO, i.e., less than 1 ppm compared to 0.1TiO, which shows a higher response rate in the concentration range of 0.3, indicating that it is an appropriate structure for gas sensors in terms of response rate, lower detection limit, and fast response/recovery time.

3.3. Sensing properties and selectivity of SnO_2 and SnO_2@TiO_2 sensors

The sensing response of the 0.2SnO and 0.2TiO sensors dependent on the concentrations of CO and HCHO gas are assessed under UV irradiation, respectively. (Fig. 7(a) and (b)) The sensing signal of both sensors shows the tendency to increase gradually at low concentration, then be saturated at higher concentration of target gases. This concentration-dependent change of resistance could be fitted by R^{-1} versus C^{-1} based on Langmuir isotherm adsorption method, where R is the response and C is the CO and HCHO concentrations, respectively, which suggest the surface adsorption capacity of target gases by quantity of active surface area [34]. The plots of 0.2SnO and 0.2TiO sensors reveal approximately linear fitting of R^{-1} versus C^{-1} (Fig. 7(c) and (d)). Other SnO and TiO sensors fabricated under various deposition pressure also exhibited the linear relationship between R^{-1} and C^{-1} in same range of target gases (Fig. S7). The lowest detection limit of SnO and TiO sensors are also evaluated in range of 1–50 ppm of CO and 0.1–10 ppm of HCHO (Fig. S8). As a result, the 0.2SnO sensor displays 12% of response to 1 ppm of CO, the 0.2TiO sensor display 3.2% of response in 0.1 ppm of HCHO which is sufficient to detect the threshold limit of indoor air quality, up to 35 ppm of CO and 0.3 ppm of HCHO, respectively. We also summarized previously reported sensors to CO and HCHO gas based on various nanostructures with different operating power in Table 1. Considering the working temperature and sensing performance, our sensor was attractive to practical application with easy and cost-effective fabrication method.

The effect of humidity on the photoactive gas-sensing capability of SnO_2 and SnO_2@TiO_2 to CO and HCHO gas was also investigated under humidity conditions of 35%, 50%, and 80% (Fig. 8). As the relative humidity (RH) increased, it was observed that the resistance of both SnO_2 and SnO_2@TiO_2 sensor decreased because the water molecules

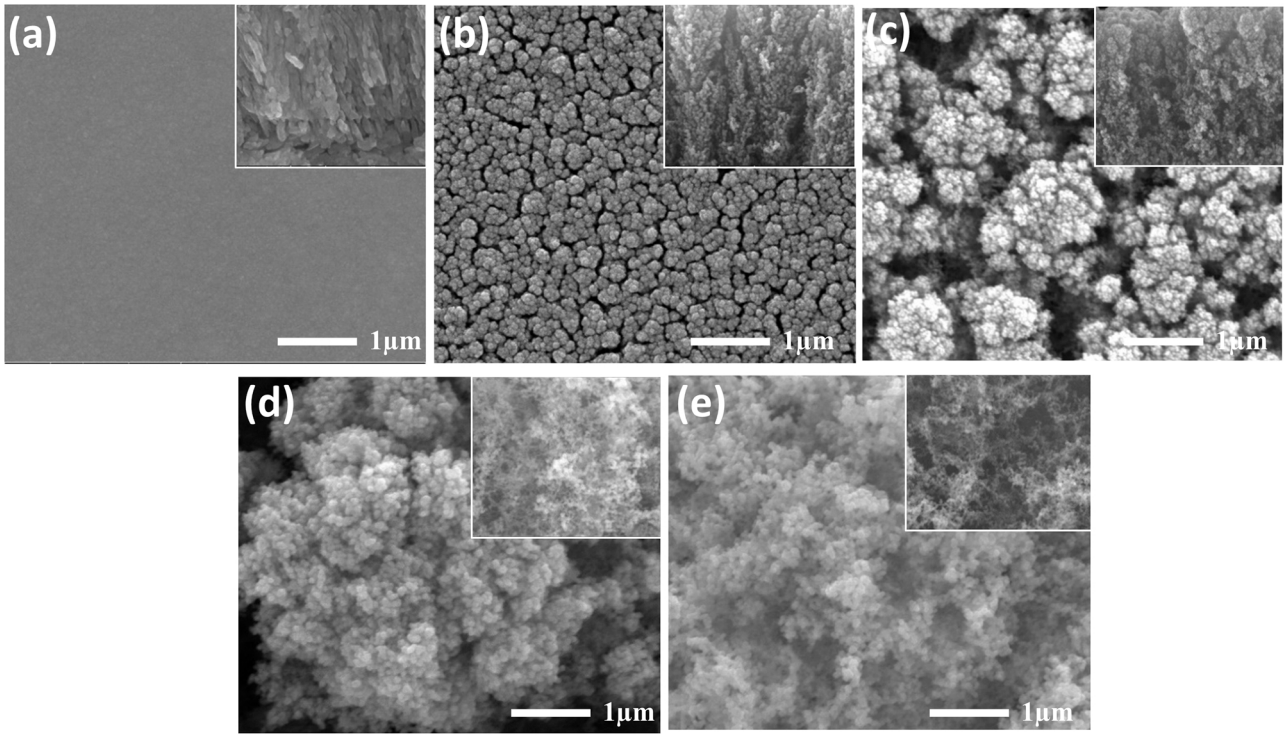

Fig. 4. FE-SEM images of SnO_2@TiO_2 surface prepared with different deposition pressure: (a) high vacuum, (b) 0.1 Torr (0.1TiO), (c) 0.2 Torr (0.2TiO), (d) 0.5 Torr (0.5TiO), and (e) 1 Torr (1TiO) (inset: cross-sectional images of porous SnO_2@TiO_2 on substrate, 100k magnification).

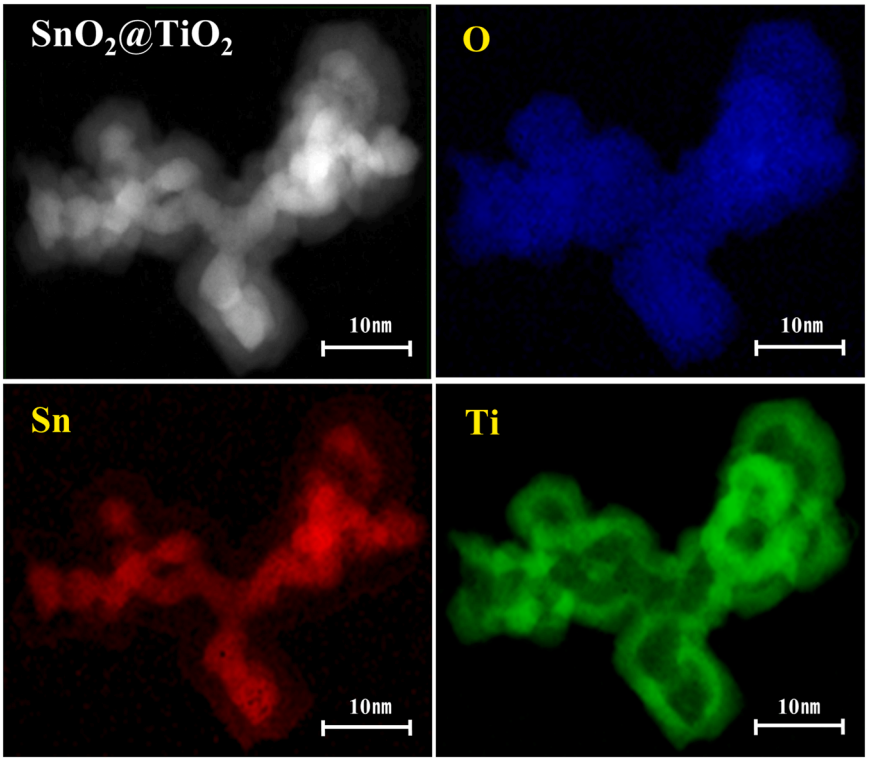

Fig. 5. Scanning transmission electron microscopy image of SnO_2@TiO_2 heterostructure and energy-dispersive spectroscopy mapping of O, Sn, Ti elements.

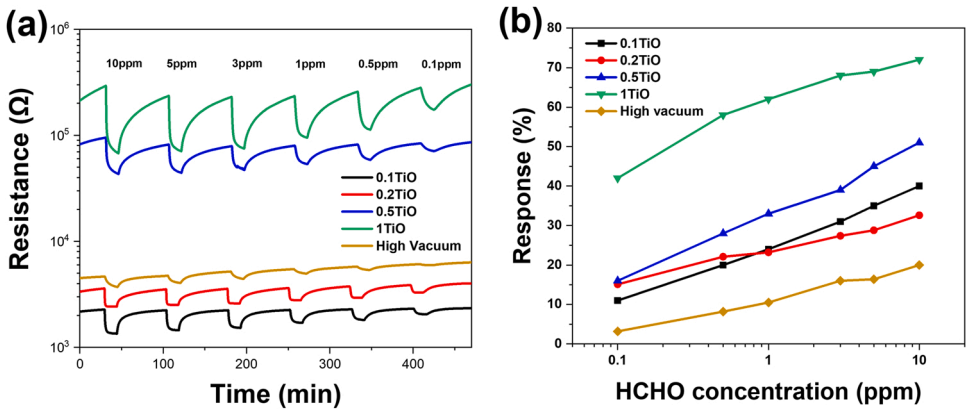

Fig. 6. (a) Transient response of porous SnO_2@TiO_2 gas sensor to different HCHO gas concentrations from 10 ppm to 0.1 ppm with various pressure conditions and (b) response (%) of porous SnO_2@TiO_2 sensor under UV-LED light (50 μW/cm^2).

could be absorbed on the surface of the sensor, thereby forming a hydroxyl group donating electrons on the surface [35–37]. The response rate of the porous SnO_2 sensor to CO gas decreased from approximately 34%, 9% and 5% in dry air to 35% and 80% in RH conditions (Fig. 8(a) and (b)). The SnO_2@TiO_2 heterostructure sensors also showed a decrease in response rate to HCHO gas from 46%, 15%, and 9% in dry air to 35% and 80% in RH (Fig. 8(c) and (d)). This is attributed to the adsorbed water molecules under humid conditions, reducing the active surface area for the gas oxidation reaction [38,39]. Notably, the response and recovery times are dramatically enhanced: the response time is improved from 810 s in dry air to 8 s for CO gas and from 144 s to 12 s for HCHO gas, owing to better charge transport and plenty of hydroxyl radicals formed under UV, which is known as an oxidant to CO and HCHO. Despite the lower response rate in humid conditions, the improvement in response and recovery time in humid conditions will be beneficial to the application of photoactive gas sensors when used with moisture and temperature sensors. The selective gas sensing under dark condition are also compared with 0.2SnO and 0.2TiO sensors to CO and HCHO, respectively. (Fig. S9) In dark condition, the 0.2SnO sensor display 3.7% of R to 30 ppm of CO gas while 0.2TiO do not exhibit the change of resistance. Moreover, the 0.2TiO sensor also displays 2.1% of R, resistance of 0.2SnO was not changed under the flow of 10 ppm HCHO gas. This result indicates not only that light illumination is required to higher sensitivity to the target gas but also that gas selective response is maintained under dark condition.

The selectivity of the photoactive gas sensor based on SnO_2 and SnO_2@TiO_2 was also evaluated using ammonia (NH_3) and acetone (C_3H_6O) in addition to CO and HCHO (Fig. 9). The responses of SnO_2 and SnO_2@TiO_2 sensors were measured at 35% RH and exposed to 10 ppm of each gas. The porous SnO_2 sensor showed a response of ~10.0% to 10 ppm of CO gas, while the responses to HCHO, NH_3, and C_3H_6O were 1.5%, 2.6%, and 1.6%, respectively. In contrast, the SnO_2 @TiO_2 sensor

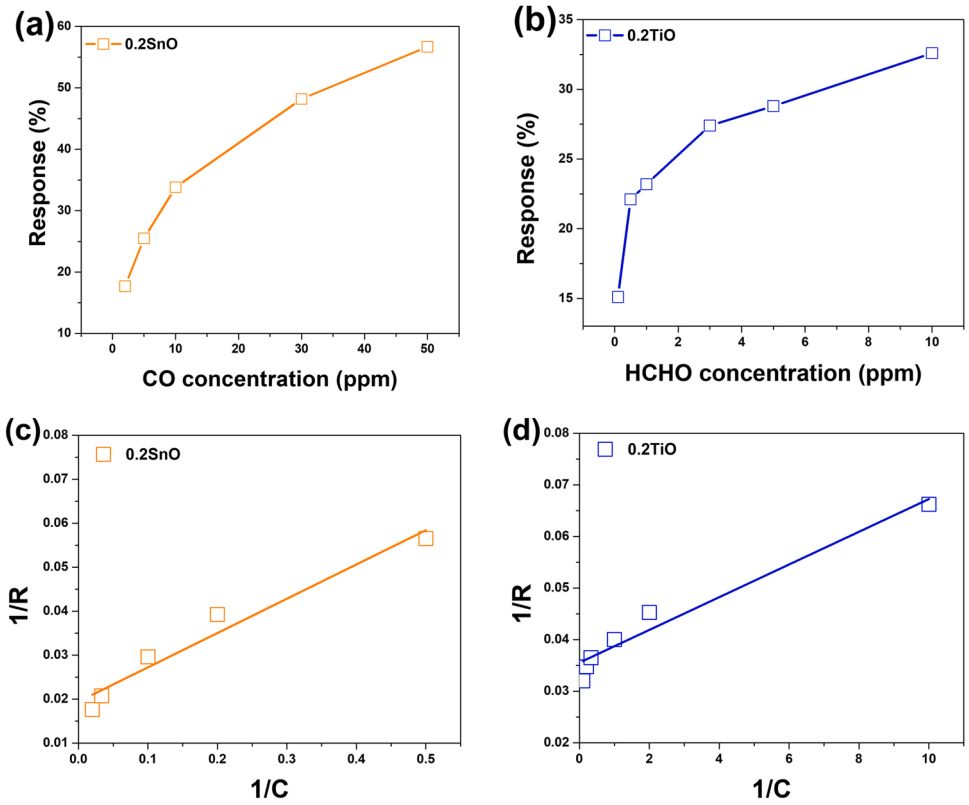

Fig. 7. The response of (a) 0.2SnO in range of 2–50 ppm of CO gas and (b) 0.2TiO sensor in range of 0.1–10 ppm of HCHO gas, respectively. The linear fitting of 1/R versus 1/C of (c) 0.2SnO and (d) 0.2TiO sensor followed Langmuir isotherm adsorption method, respectively.

Table 1
Performance of various metal oxide-based gas sensors for CO or HCHO detection.

Materials	Structure	Target gas	T (℃) or Voltage (V)	UV	Concentration (ppm)	R_a/R_g	LOD (ppm)	Ref.
SnO_2	Nanosheet	HCHO	200 ℃	–	100	79.5	1	[48]
Zn_2SnO_4/SnO_2	Hierarchical octahedral-like	HCHO	200 ℃	–	100	60	2	[49]
SnO_2/ZnO	Heterostructure	HCHO	–	UV	10	30	0.1	[50]
TiO_2/SnO_2	Nanosphere	HCHO	–	UV	10	20	0.1	[51]
Au-SnO_2/ZnO	Nanowire	CO	20 V	–	50	1.6	0.1	[52]
Pt-SnO_2	Nanoneedle	CO	250 ℃	–	100	23.2	1	[53]
Ni doped SnO_2	Nanocomposite	CO	280 ℃	–	300	25.1	1	[54]
Au-WS_2	Nanoflake	CO	2 V	–	50	1.4	1	[55]
SnO_2	**Nanocomposite**	**CO**	–	**UV**	**50**	**56.7**	**0.1**	**This work**
SnO_2@TiO_2	**Heterostructure**	**HCHO**	–	**UV**	**10**	**32.7**	**1**	**This work**

exhibited a 15.1% response to HCHO, whereas the responses to CO, NH_3, and C_3H_6O were 3.5%, 2.8%, and 1.5%, respectively, thereby achieving specificity to HCHO. The selective detection of CO and HCHO in the SnO_2 and SnO_2@TiO_2 sensors was compared with the concentration of the target gas in detail (Fig. S10). This result indicates that the oxidation energy levels of HCHO and CO gas are well-matched with the adsorbed oxygen energy levels of TiO_2 and SnO_2, respectively, thus inducing selective oxidation of specific gases.

The absorption and reaction, including oxidation and reduction of gas molecules on the surface of the material, significantly impact the response and selectivity of gas sensors. Conventional resistor-type sensors require a specific temperature range depending on the material to generate a special type of ionized oxygen, such as O^- and O_2^-, for the oxidation of the target gas [40,41]. In photoactive gas sensors, UV irradiation replaces high-temperature activation to generate excitons and react with adsorbed oxygen and hydroxyl groups [42–44]. In this study, the selective detection of each gas is attributed to different types of reactive oxygen species, as well as the matching energy level between the oxidation of gas and the conduction band. To detect CO, the adsorbed oxygen and hydroxyl groups are converted to O^- under UV irradiation on the surface of SnO_2. This reactive oxygen level on the surface of SnO_2 is well-matched with the oxidation energy level of CO. Therefore, the reactive oxygen species O^- oxidizes CO to CO_2, thus generating electrons and reducing the resistance of the sensor [45] (Fig. 10(a)). The detailed reaction is as follows:

$$CO\ (gas) + O^-\ (ads,\ SnO_2)\ (hv) \rightarrow CO_2\ (gas) + e^- \quad (1)$$

In contrast, the adsorbed oxygen species on the surface of TiO_2 are converted to O_2^- by excitons generated under UV irradiation. The redox energy level of HCHO, which is higher than the conduction band of SnO_2, matches well with the conduction band of TiO_2 (Fig. 10(b)). Therefore, the reactive oxygen on the TiO_2 oxidize HCHO and generate electron back in TiO_2, under UV irradiation [46,47] like below equation:

$$HCHO\ (gas) + O_2^-\ (ads,\ TiO_2)\ (hv) \rightarrow CO_2 + H_2O + e^- \quad (2)$$

Notably, the SnO_2@TiO_2 heterostructure exhibits a faster response time to HCHO than SnO_2 to CO. Because the heterojunction between TiO_2 and SnO_2 promotes charge transfer due to the equilibrium of the

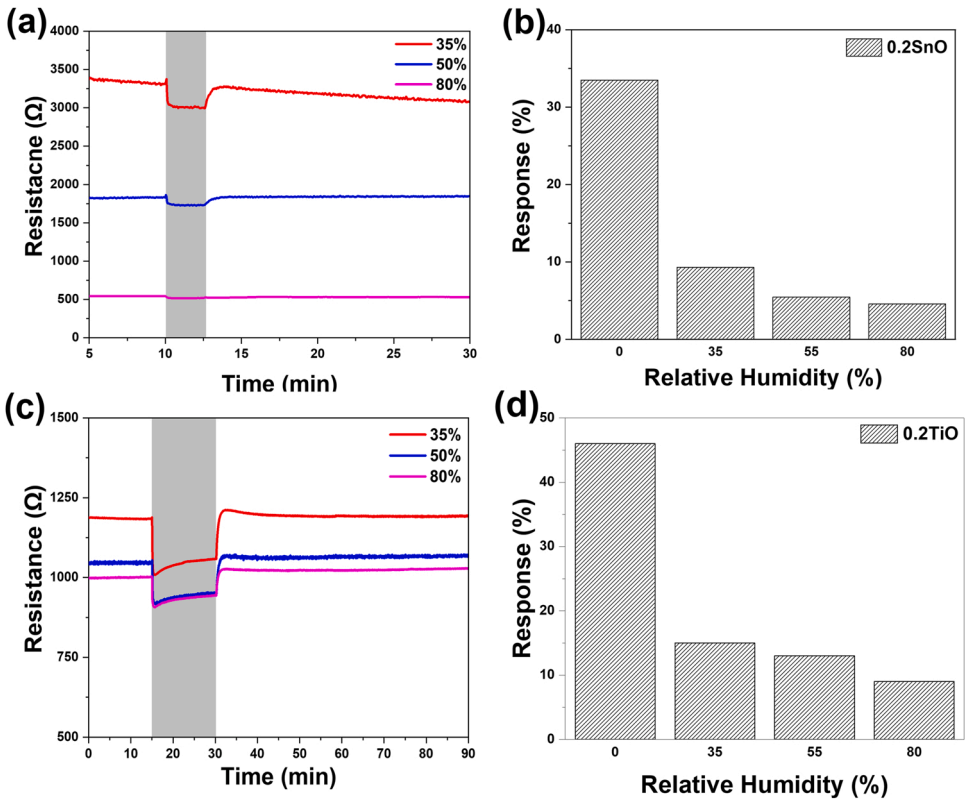

Fig. 8. The transient response of (a) porous 0.2SnO sensor to 10 ppm of CO gas and (c) 0.2TiO sensor to 10 ppm of HCHO gas and corresponding response (%) of (b) 0.2SnO and (d) 0.2TiO sensors under the humid condition with relative humidity of 35%, 50%, and 80%.

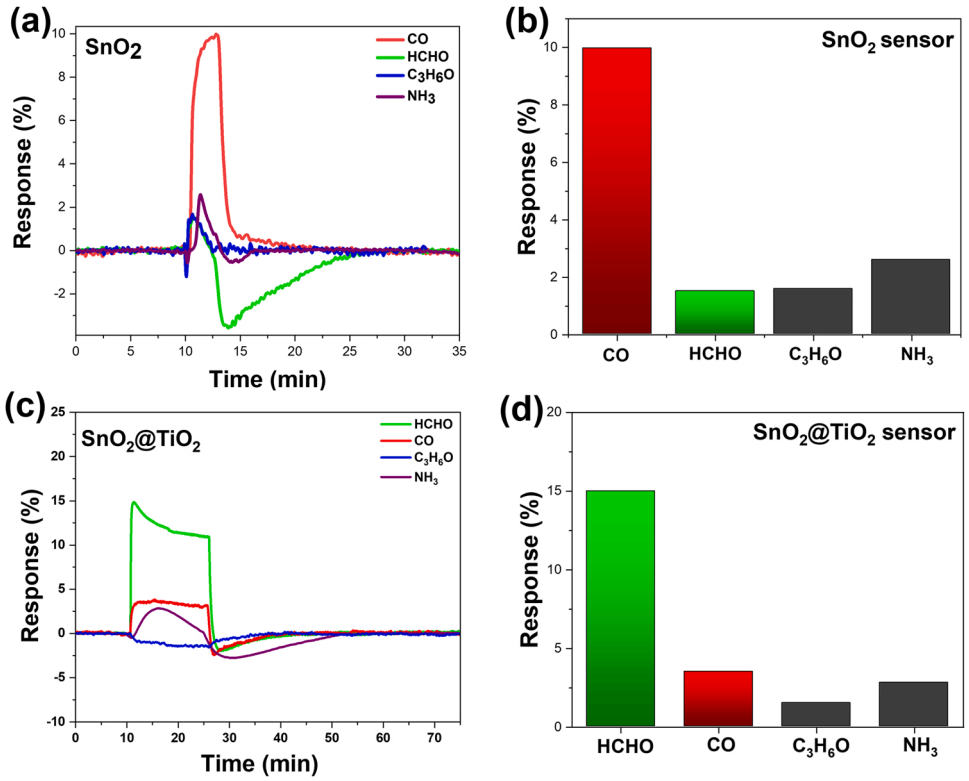

Fig. 9. The transient response of (a) SnO_2 and (b) SnO_2@TiO_2 sensors with various gases as CO, HCHO, C_3H_6O, and NH_3 and comparison response rate of (b) SnO_2 and (d) SnO_2@TiO_2.

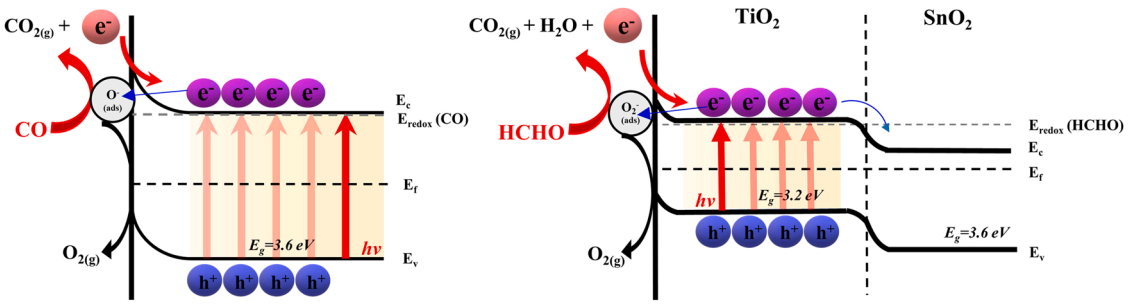

Fig. 10. The sensing mechanism of (a) SnO_2 and (b) SnO_2@TiO_2 sensors. The different types of ionized oxygen species adsorbed on the surface selectively oxidize CO and HCHO gas.

Fermi level, the transport of charge carriers generated by reaction with the target gas is enhanced in SnO_2@TiO_2, which is in good agreement with the lower resistance after ALD deposition.

4. Conclusion

In summary, highly porous SnO_2 and SnO_2@TiO_2 sensors were successfully synthesized by facile Ar flow thermal evaporation and ALD for photoactive gas sensor applications. The obtained SnO_2 is controlled in pore and ligament sizes with the Ar flow pressure during thermal evaporation, and a conformal SnO_2@TiO_2 heterostructure is achieved by the ALD process. The photoactive gas-sensing properties of the porous SnO_2 and SnO_2@TiO_2 heterostructures were investigated for CO and HCHO gas under UV irradiation at room temperature (27 °C). The SnO_2- and SnO_2@TiO_2-based photoactive gas sensor exhibited a good response to CO in the range of 2–50 ppm and HCHO in the range of 0.1–10 ppm, respectively, at room temperature, as well as selective detection of CO and HCHO. The existence of a TiO_2 layer with a conduction band that is well-matched with the redox energy level of HCHO enables the porous SnO_2 structure not only to selectively detect HCHO but also to enhance the response time by promoting charge transport. Moreover, the effects of the humid conditions and other gases, such as NH_3 and C_3H_6O, were investigated for reliable gas sensors. This finding demonstrates the possibility of achieving high sensitivity and gas selectivity in photoactive gas sensors operating at room temperature to mitigate the drawbacks of resistor-type gas sensors at high temperatures. Moreover, our results provide a method for manufacturing a photoactive gas sensor that can be applied to various target gases along with a wide range of materials available in our process.

CRediT authorship contribution statement

Sungjin Kim: Investigation, Validation, Data curation, Formal analysis, Writing – original draft. **Deok-hyun Cho:** Investigation, Validation, Formal analysis. **Hyeon-Kyung Chang:** Investigation, Formal analysis. **Ho-Nyun Lee:** Resources, Data curation. **Hyun-Jong Kim:** Investigation, Data curation. **Tae Joo Park:** Supervision, Writing – review & editing. **Young Min Park:** Conceptualization, Supervision, Writing – review & editing, Project administration.

Declaration of Competing Interest

The authors declare that they have no known competing financial interests or personal relationships that could have appeared to influence the work reported in this paper.

Acknowledgment

This research was financially supported by the Basic Research Program of the National Research Foundation of Korea, South Korea (Project No. NRF-2020R1F1A1067830).

Appendix A. Supporting information

Supplementary data associated with this article can be found in the online version at doi:10.1016/j.snb.2022.131486.

References

[1] S.M. Majhi, A. Mirzaei, H.W. Kim, S.S. Kim, T.W. Kim, Recent advances in energy-saving chemiresistive gas sensors: a review, Nano Energy 79 (2021), 105369.
[2] A. Bag, N.-E. Lee, Recent advancements in development of wearable gas sensors, Adv. Mater. Technol. 6 (2021), 2000883.
[3] P.G. Choi, N. Izu, N. Shirahata, Y. Masuda, Improvement of sensing properties of SnO_2 gas sensor by tuning of exposed crystal face, Sens. Actuators B. Chem. 296 (2019), 126655.
[4] M. Tonezzer, Selective gas sensor based on one single SnO_2 nanowire, Sens. Actuators B. Chem. 288 (2019) 53–59.
[5] D. Nagmani, A. Pravarthana, T.G. Tyagi, W. Jagadale, D.K.Aswal Prellier, Highly sensitive and selective H_2S gas sensor based on TiO_2 thin films, Appl. Surf. Sci. 549 (2021), 149281.
[6] A.V. Lashkov, F.S. Fedorov, M. Yu, Vasilkov, A.V. Kochetkov, I.V. Belyaev, I. A. Plugin, A.S. Varezhnikov, A.N. Filipenko, S.A. Romanov, A.G. Nasibulin, G. Korotcenkov, V.V. Sysoev, The Ti wire functionalized with inherent TiO_2 nanotubes by anodization as one-electrode gas sensor: a proof-of-concept study, Sens. Actuators B. Chem. 306 (2020), 127615.
[7] G. Li, Z. Sun, D. Zhang, Q. Xu, L. Meng, Y. Qin, Mechanism of sensitivity enhancement of a ZnO nanofilm gas sensor by UV light illumination, ACS Sens. 4 (2019) 1577–1585.
[8] T.-J. Hsueh, C.-H. Peng, W.-S. Chen, A transparent ZnO nanowire MEMs gas sensor prepared by an ITO micro-heater, Sens. Actuators B Chem. 304 (2020), 127319.
[9] H.-L. Yu, J. Wang, B.Z. Zheng, B.-W. Zhang, L.-Q. Liu, Y.-W. Zhou, C. Zhang, X.-L. Xue, Fabrication of single crystalline WO_3 nano-belts based photoelectric gas sensor for detection of high concentration ethanol gas at room temperature, Sens. Actuator A Phys. 303 (2020), 111865.
[10] B. Bouchikhi, T. Chludziński, T. Saidi, J. Smulko, N.E. Bari, H. Wen, R. Ionescu, Formaldehyde detection with chemical gas sensors based on WO_3 nanowires decorated with metal nanoparticles under dark conditions and UV light irradiation, Sens. Actuators B Chem. 320 (2020), 128331.
[11] D.N. Oosthuizen, D.E. Motaung, H.C. Swart, Gas sensors based on CeO_2 nanoparticles prepared by chemical precipitation method and their temperature-dependent selectivity towards H_2S and NO_2 gases, Appl. Surf. Sci. 505 (2020), 144356.
[12] C. Wang, L. Yin, L. Zhang, D. Xiang, R. Gao, Metal oxide gas sensors: sensitivity and influencing factors, Sensors 10 (2010) 2088–2106.
[13] A. Ghosh, C. Zhang, S.Q. Shi, H. Zhang, High-temperature gas sensors for harsh environment applications: a review, Clean. – Soil Air Water 47 (2019), 1800491.
[14] Z.-H. Ma, R.-T. Yu, J.-M. Song, Facile synthesis of Pr-doped In_2O_3 nanoparticles and their high gas sensing performance for ethanol, Sens. Actuators B Chem. 305 (2020), 127377.
[15] T.-H. Kim, S.-Y. Jeong, Y.K. Moon, J.-H. Lee, Dual-mode gas sensor for ultrasensitive and highly selective detection of xylene and toluene using Nb-doped NiO hollow spheres, Sens. Actuators B Chem. 301 (2019), 127140.
[16] X. Wang, T. Wang, G. Si, Y. Li, S. Zhang, X. Deng, X. Xu, Oxygen vacancy defects engineering on Ce-doped a-Fe_2O_3 gas sensor for reducing gases, Sens. Actuators B Chem. 302 (2020), 127165.
[17] H.-J. Le, D.V. Dao, Y.-T. Yu, Superfast and efficient hydrogen gas sensor using $PdAu_{alloy}$@ZnO core-shell nanoparticles, J. Mater. Chem. A. 8 (2020) 12968.
[18] R. Zhao, T. Wang, M. Zhao, C. Xia, Y. An, S. Wei, X. Dai, External electric field and strains facilitated nitrogen dioxide gas sensing properties on 2D monolayer and bilayer SnS_2 nanosheet, Appl. Surf. Sci. 491 (2019) 128–137.
[19] M.A. Han, H.-J. Kim, H.C. Lee, J.-S. Park, H.-N. Lee, Effects of porosity and particle size on the gas sensing properties of SnO_2 films, Appl. Surf. Sci. 481 (2019) 133–137.
[20] S. Zhang, M. Yang, K. Liang, A. Turak, B. Zhang, D. Meng, C. Wang, F. Qu, W. Cheng, M. Yang, An acetone gas sensor based on nanosized Pt-loaded Fe_2O_3 nanocubes, Sens. Actuators B. Chem. 290 (2019) 56–67.

[21] Y.M. Sabri, A.E. Kandjani, S.S.A.A.H. Rashid, C.J. Harrison, S.J. Ippolito, S. K. Bhargava, Soot template TiO_2 fractals as a photoactive gas sensor for acetone detection, Sens. Actuators B. Chem. 275 (2018) 215–222.
[22] G. Li, Z. Sun, D. Zhang, Q. Xu, L. Meng, Y. Qin, Mechanism of sensitivity enhancement of a ZnO nanofilm gas sensor by UV light illumination, ACS Sens. 4 (2019) 1577–1585.
[23] E. Espid, F. Taghipour, Development of highly sensitive ZnO/In_2O_3 composite gas sensor activated by UV-LED, Sens. Actuators B. Chem. 241 (2017) 828–839.
[24] M.E. Franke, T.J. Koplin, U. Simon, Metal and metal oxide nanoparticles in chemiresistors: does the nanoscale matter? Small 2 (2006) 36–50.
[25] J.W. Kim, Y. Porte, K.Y. Ko, H. Kim, J.M. Myoung, Micropatternable double-faced ZnO nanoflowers for flexible gas sensor, ACS Appl. Mater. Interfaces 9 (2017) 32876–32886.
[26] Y. Zhang, W. Zeng, New insight into gas sensing performance of nanoneedle-assembled and nanosheet-assembled hierarchical NiO nanoflowers, Mater. Lett. 195 (2017) 217–219.
[27] Y.M. Park, S.H. Hwang, H. Lim, H.-N. Lee, H.-J. Kim, Scalable and versatile fabricataion of metallic nanofoam films with controllable nanostructure using Ar-assisted thermal evaporation, Chem. Mater. 33 (2021) 205–211.
[28] J.-P. Ahn, S.-H. Kim, J.-K. Park, M.-Y. Huh, Effect of orthorhombic phase on hydrogen gas sensing property of thick-film sensors fabricated by nanophase tin dioxide, Sens. Actuators B. Chem. 94 (2003) 125–131.
[29] W.K. Choi, H. Sung, K.H. Kim, J.S. Cho, S.C. Choi, H.-J. Jung, et al., Oxidation process from SnO to SnO_2, J. Mater. Sci. Lett. 16 (1997) 1551–1554.
[30] Z.R. Dai, Z.W. Pan, Z.L. Wang, Growth and structure evolution of novel tin oxide diskettes, J. Am. Chem. Soc. 124 (2002) 8673–8680.
[31] H.-K. Chang, D.-S. Ko, D.-H. Cho, S. Kim, H.-N. Lee, H.-J. Kim, T.J. Park, Y.M. Park, Enhanced response of the photoactive gas sensor on formaldehyde using porous SnO_2@TiO_2 heterostructure driven by gas-flow thermal evaporation and atomic layer deposition, Ceram. Int. 47 (2020) 5985–5992.
[32] Q. Zhang, P. Liu, C. Miao, Z. Chen, C.L. Wu, C.-H. Shek, Formation of orthorhombic SnO_2 originated from lattice distortion by Mn-doped tetragonal SnO_2, RSC Adv. 5 (2015) 39285–39290.
[33] L. Zhang, H.B. Wu, X. Wen Lou, Growth of SnO_2 nanosheet arrays on various conductive substrates as integrated electrodes for lithium-ion batteries, Mater. Horiz. 1 (2014) 133–138.
[34] Y. Xia, J. Wang, L. Xu, X. Li, S. Huang, A room-temperature methane sensor based on Pd-decorated ZnO/rGO hybrids enhanced by visible light photocatalysis, Sens. Actuators B. Chem. 304 (2020), 127334.
[35] K. Suematsu, N. Ma, K. Watanabe, M. Yuasa, T. Kida, K. Shimanoe, Effect of humid aging on the oxygen adsorption in SnO_2 gas sensors, Sensors 18 (2018) 254.
[36] X.-Y. Zhang, R.-H. Ma, L.-S. Li, Y.-T. Fan, S.-Y. Yang, Zhang, A room-temperature ultrasonic hydrogen sensor based on a sensitive layer of reduced graphene oxide, Sci. Rep. 11 (2021) 2404.
[37] Y. Cheng, B. Ren, K. Xu, I. Jeerapan, H. Chen, Z. Li, J.Z. Ou, Recent progress in intrinsic and stimulated room-tmeperature gas sensors enabled by low-dimensional materials, J. Mater. Chem. C. 9 (2021) 3026–3051.
[38] L. Liu, X. Li, P.K. Dutta, J. Wang, Room temperature impedance spectroscopy-based sensing of formaldehyde with porous TiO_2 under UV illumination, Sens. Actuators B. Chem. 185 (2013) 1–9.
[39] C. Wang, L. Yin, L. Zhang, D. Xiang, R. Gao, Metal oxide gas sensors: sensitivity and influencing factors, Sensors 10 (2010) 2088–2106.
[40] N. Yamazoe, Toward innovations of gas sensor technology, Sens. Actuators B. Chem. 108 (2005) 2–14.
[41] S. Mishra, C. Ghanshyam, N. Ram, R.P. Bajpai, R.K. Bedi, Detection mechanism of metal oxide gas sensor under UV radiation, Sens. Actuators B. Chem. 97 (2004) 387–390.
[42] E. Comini, A. Cristalli, G. Faglia, G. Sberveglieri, Light enhanced gas sensing properties of indium oxide and tin dioxide sensors, Sens. Actuators B. Chem. 65 (2000) 260–263.
[43] K. Anothainart, M. Burgmair, A. Karthigeyan, M. Zimmer, I. Eisele, Light enhanced NO_2 gas sensing with tin oxide at room temperature: conductance and work function measurements, Sens. Actuators B. Chem. 93 (2003) 580–584.
[44] X. Li, X. Li, J. Wang, S. Lin, Highly sensitive and selective room-temperature formaldehyde sensors using hollow TiO_2 microspheres, Sens. Actuators B. Chem. 219 (2015) 158–163.
[45] X. Wang, H. Qin, Y. Chen, J. Hu, Sensing mechanism of SnO2 (110) surface to CO: density functional theory calculations, J. Phys. Chem. C. 118 (2014) 28548–28561.
[46] Z. Han, Y. Qi, Z. Yang, H. Han, Y. Jiang, W. Du, X. Zhang, J. Zhang, Z. Dai, L. Wu, C. Fletcher, Z. Wang, J. Liu, G. Lu, F. Wang, Recent advances and perspectives on construcing metal oxide semiconductor gas sensing materials for efficient formaldehyde detection, J. Mater. Chem. C. 8 (2020) 13169–13188.
[47] S. Sun, J. Ding, J. Bao, C. Gao, Z. Qi, C. Li, Photocatalytic oxidation of gaseous formaldehyde on TiO_2: an in situ DRIFTS study, Catal. Lett. 137 (2010) 239–246.
[48] R. Xu, L.-X. Zhang, M.-W. Li, Y.-Y. Yin, J. Yin, M.-Y. Zhu, J.-J. Chen, Y. Wang, L.-J. Bie, Ultrathin SnO_2 nanosheets with dominant high-energy {001} facets for low temperature formaldehyde gas sensor, Sens. Actuators B. Chem. 289 (2019) 186–194.
[49] S. Shu, M. Wang, W. yang, S. Liu, Synthesis of surface layered hierarchical octahedral-like structured Zn_2SnO_4/SnO_2 with excellent sensing properties toward HCHO, Sens. Actuators B. Chem. 243 (2017) 1171–1180.
[50] J. Jiang, L. Shi, T. Xie, D. Wang, Y. Lin, Study on the gas-sensitive properties for formaldehyde based on SnO_2-ZnO heterostructure in UV excitation, Sens. Actuators B. Chem. 254 (2018) 863–871.
[51] S. Zhang, L. Zhao, B. Huang, X. Li, UV-activated formaldehyde sensing properties of hollow TiO_2@SnO_2 heterojunctions at room temperature, Sens. Actuators B. Chem. 319 (2020), 128264.
[52] J.-H. Kim, A. Mirzaei, H.W. Kim, S.S. Kim, Low power-consumption CO gas sensors based on Au-functionalized SnO_2-ZnO core-shell nanowires, Sens. Actuators B. Chem. 267 (2018) 597–607.
[53] Q. Zhou, L. Xu, A. Umar, W. Chen, R. Kumar, Pt nanoparticles decorated SnO_2 nanoneedles for efficient CO gas sensing applications, Sens. Actuators B. Chem. 256 (2018) 656–664.
[54] Q. Zhou, W. Chen, L. Xu, R. Kumar, Y. Gui, Z. Zhao, C. Tang, S. Zhu, Highly sensitive carbon monoxide (CO) gas sensors based on Ni and Zn doped SnO_2 nanomaterials, Ceram. Int. 44 (2018) 4392–4399.
[55] J.-H. Kim, A. Miraei, H.W. Kim, S.S. Kim, Flexible and low power CO gas sensor with Au-functionalized 2D WS_2 nanoflakes, Sens. Actuators B. Chem 313 (2020) 128040.

Sungjin Kim completed his M.S. degree from Sungkyunkwan University. During his mater course, he studied organic compound of channel material of OTFT based on organic chemistry. He joined the joint Ph.D. Program of Korea Institute of Industrial Technology (KITECH) and Hanyang University in 2017. He is now studying thin film deposition and its applications in energy materials.

Deok-Hyun Cho received his B.S. degree in Department of Chemical Engineering and Biotechnology from Korea Polytechnic University. He is currently a graduate student in Department of Materials Science and Chemical Engineering, Hanyang University. He joined the joint M.S. Program of Korea Institute of Industrial Technology (KITECH) and Hanyang University in 2018. He is now studying thin film deposition and its applications in photo-actived gas sensors.

Hyeon-Kyung Chang received her B.S. degree in Department of High Polymer Engineering from Inha University. She is currently a graduate student in Department of Materials Science and Chemical Engineering, Hanyang University. She joined the joint M.S. Program of Korea Institute of Industrial Technology (KITECH) and Hanyang University in 2019. She is now studying thin film deposition and its applications in photo-actived gas sensors under supervision of Dr. Young Min Park and Prof. Tae Joo Park.

Ho-Nyun Lee is a principal researcher in surface technology group, Korea Institute of Industrial Technology. He received his Ph.D in material science from Korea Advanced Institute of Science and Technology (KAIST) in 2001. Before joining to current group, he worked at LG electronics and LG display as senior researcher for 7 years. His main areas of research interest includes thin film process and surface functionalization.

Hyun-Jong Kim received his Ph.D. in Chemical Engineering in 2004 from Yonsei University (Korea). After postdoctoral research at National Institute of Advanced Industrial Science & Technology (AIST), he joined the Nano-surface technology team at Korea Institute of Industrial Technology (KITECH), where he is currently a principal researcher of Surface R&D group. His research interests include electrocatalysts and energy storage materials.

Tae Joo Park received the B.Eng. and Ph.D. degrees in Materials Science and Engineering from Seoul National University, Seoul, Korea, in 2002 and 2008, respectively. His research at Seoul National University covered electrical and chemical characterizations of advanced gate stacks with metal gate/high-k/high-mobility channel and nonvolatile memory applications and thin-film growth using atomic-layer deposition. From 2008–2010, he was a Research Scientist with the Department of Materials Science and Engineering at the University of Texas at Dallas, Richardson, where he was engaged in advanced nanoelectronic devices based on organic/inorganic thin films, graphene layer growth, and in situ XPS analysis of thin films. In 2011, he joined Department of Materials Science and Chemical Engineering at Hanyang University, where he is now an Associate Professor. He has published more than 100 papers in technical journals with more than 180 presentations in international conferences. His research interests include energy harvesting/storage systems and nanoelectronic devices.

Young Min Park is a principal researcher at Korea Institute of Industrial Technology (KITECH) in Korea. He received his PhD in Materials Science and Engineering from Stanford University, California, USA in 2012. From 2013–2014 and 2014–2016, he was a senior researcher in Samsung Corning Precision Materials and Samsung Electronics, respectively. In 2016, he joined Surface Technology Group at Korea Institute of Industrial Technology (KITECH). He has published more than 25 papers in technical journals. His current research interests focus on nano-porous materials and its application for sensor, energy conversion and biomedical diagnostics.